Strong-coupling expansions for the anharmonic Holstein model and for the Holstein-Hubbard model

J. K. Freericks
Department of Physics, Georgetown University, Washington, D.C. 20057-0995

G. D. Mahan
Department of Physics and Astronomy, University of Tennessee, Knoxville, Tennessee 37996-1200
and Solid State Division, Oak Ridge National Laboratory, P.O. Box 2008, Oak Ridge, Tennessee 37831-6030

(Received 1 April 1996)

A strong-coupling expansion is applied to the anharmonic Holstein model and to the Holstein-Hubbard model through fourth order in the hopping matrix element. Mean-field theory is then employed to determine transition temperatures of the effective (pseudospin) Hamiltonian. We find that anharmonic effects are not easily mimicked by an on-site Coulomb repulsion and that anharmonicity strongly favors superconductivity relative to charge-density-wave order. Surprisingly, the phase diagram is strongly modified by relatively small values of the anharmonicity. [S0163-1829(96)00737-0]

I. INTRODUCTION

The interaction of conduction electrons in a solid with lattice vibrations is described by the so-called electron-phonon problem. Migdal[1] and Eliashberg[2] pioneered the study of such interacting fermion-boson systems in the limit where the phonons are all harmonic and the phonon energy scale is much smaller than the electronic energy scale. Vertex corrections can be neglected in this case[1] and a self-consistent theory can be constructed that is exact in the limit of weak coupling; the theory is an expansion in powers of the coupling strength multiplied by the ratio of the phonon energy scale to the electronic energy scale.

But phonons in real materials are never purely harmonic—higher-order (anharmonic) contributions to the phonon potential are always present. This phonon anharmonicity is responsible for many different physical effects in solids. For example, thermal expansion arises purely from anharmonic effects—a harmonic crystal does not change its volume upon heating. Such anharmonic effects have been treated in an approximate fashion: In the quasiharmonic approximation[3] only the effect of thermal expansion is taken into account by postulating that the phonon frequencies have a dependence upon the volume of the crystal, as described by the Grüneisen parameter; in the self-consistent harmonic approximation[4] the harmonic force constants are self-consistently replaced by their thermal averages over all possible motions of the other atoms—it is used to describe systems with strong anharmonicity; finally, in the pseudoharmonic approximation[5] both thermal expansion effects and phonon-phonon interactions are taken into account by employing the quasiharmonic approximation plus a perturbative expansion in the phonon-phonon interaction. Superconducting transition temperatures have also been studied, with the result that anharmonicity does not enhance the transition temperature in the weak- to moderate-coupling regime where Eliashberg theory applies.[6] But an exact treatment of lattice anharmonicity is difficult from a theoretical point of view because an anharmonic ''perturbation'' is never a small perturbation; the phonon wave functions are always dominated by the anharmonic terms in the potential as the phonon coordinate becomes large. Even the qualitative effects of lattice anharmonicity on superconductivity are not well understood. All that is known rigorously about the anharmonic electron-phonon problem is that the ground state must contain a spin singlet[7] for even numbers of electrons on a finite lattice.

Much progress can be made, however, in the limit of strong coupling (the electron-phonon interaction is much larger than the hopping integral of the electrons), where the electrons strongly bind together into preformed pairs (called bipolarons) and the ground state of the system is highly degenerate. Degenerate perturbation theory (in the kinetic energy of the electrons) about this bipolaronic ground state produces an expansion in inverse powers of the coupling strength. This theory has been exhaustively analyzed to second order in the hopping[8] and has recently been studied to fourth order in the hopping.[9] In this contribution, the fourth-order calculations are extended to include both anharmonic phonons and a direct electron-electron repulsion.

The simplest electron-phonon model that includes both anharmonic effects and direct electron-electron repulsion is the anharmonic Holstein-Hubbard model[10,11] in which the conduction electrons interact with themselves and with local phonon modes:

$$H=-\sum_{i,j,\sigma} t_{ij}c_{i\sigma}^{\dagger}c_{j\sigma}+\sum_i (gx_i-\mu)(n_{i\uparrow}+n_{i\downarrow}) + U_C\sum_i n_{i\uparrow}n_{i\downarrow}+\frac{1}{2M}\sum_i p_i^2+\frac{1}{2}M\Omega^2\sum_i x_i^2 + \alpha_{\mathrm{anh}}\sum_i x_i^4, \tag{1}$$

where $c_{i\sigma}^{\dagger}$ ($c_{i\sigma}$) creates (destroys) an electron at site i with spin σ, $n_{i\sigma}=c_{i\sigma}^{\dagger}c_{i\sigma}$ is the electron number operator, and x_i (p_i) is the phonon coordinate (momentum) at site i. The

hopping of electrons between lattice sites i and j is governed by the hopping matrix element t_{ij} (t_{ij} is a Hermitian matrix).

The local phonon has a mass M and a frequency Ω associated with it; the combination $\kappa := M\Omega^2$ is a spring constant that measures the stored energy per unit length squared in the phonon coordinate. The anharmonic contribution to the phonon potential energy is chosen to be a quartic in the phonon coordinate with a strength $\alpha_{\rm anh}$. The electron-phonon interaction strength is parametrized by an energy per unit length and is denoted g. A useful combination of fundamental parameters is the bipolaron binding energy (in the harmonic limit with $U_C=0$)

$$U := -\frac{g^2}{M\Omega^2} = -\frac{g^2}{\kappa}, \tag{2}$$

which determines the energy scale for the effective electron-electron interaction mediated by the phonons. This attraction competes with the direct Coulomb repulsion denoted by U_C. The chemical potential is μ.

The hopping matrix elements t_{ij} are used to define the energy scale. The choice $t_{1\rm NN} =: t^*/2\sqrt{d}$ for the nearest-neighbor hopping matrix element, with $t^*=1$ and d the dimensionality of the lattice, is made so as to have a well-defined limit when $d\to\infty$. The mass is then set equal to 1 ($M=1$), leaving U, U_C, $\alpha_{\rm anh}$, and Ω as free parameters. The strong coupling expansion is a perturbative expansion in the hopping terms of Eq. (1) and is valid when the bipolaron binding energy is much larger than the electronic hopping integral. Another important parameter in the strong coupling limit is the polaron band-narrowing parameter denoted by $S := |U|/\Omega$.

The original Holstein Hamiltonian corresponds to the case $\alpha_{\rm anh}=U_C=0$. Both the harmonic Holstein model and the harmonic Holstein-Hubbard model have been solved exactly in the limit of infinite dimensions via quantum Monte Carlo simulation.[12,13] These models display charge-density-wave (CDW) order near half-filling and superconductivity (SC) away from half-filling. As the phonon frequency is increased, the SC is favored relative to the CDW order. However, in the strong coupling limit, CDW order is favored over SC because of the band-narrowing effect of the bipolaron. The quantum Monte Carlo simulations also found that the effective phonon potential (determined after integrating out the effects of the electrons) generically acquires a double-well structure, signifying the formation of a bipolaron and indicating that a strong coupling expansion should be accurate even down to moderate values of the coupling strength. This has proved to be true for the harmonic case[9] and is likely to also hold over a more restricted region for the anharmonic case.

An initial analysis of the anharmonic model in the strong-coupling limit ($t_{ij}=0$) can be made by using the Born-Oppenheimer approximation:[14] The phonon frequency is assumed to be smaller than any of the other energy scales, and so the phonons can be approximated by static lattice distortions corresponding to the minimum of the phonon potential energy. Since the phonons couple linearly to the electronic charge, the equilibrium phonon coordinate varies when there are zero, one, or two electrons on a site. The origin $x_0=0$ is chosen to correspond to the case with no electrons on a site. Then x_1 and x_2 denote the equilibrium coordinates with one or two electrons on a lattice site. In the harmonic case the relative distances x_1-x_0 and x_2-x_1 are identical, which is a requirement for particle-hole symmetry. When a lattice anharmonicity is turned on, the equilibrium phonon coordinates with one and two electrons on a lattice site all move toward the origin, but the relative distances are no longer symmetric; rather, the distance x_2-x_1 becomes significantly smaller than x_1-x_0, as can be seen by calculating the perturbative shift in the equilibrium coordinates[14] as a function of the anharmonicity $\alpha_{\rm anh}$:

$$x_0=0, \quad x_1 = -\frac{g}{M\Omega^2} + \frac{4\alpha_{\rm anh} g^3}{M^4\Omega^8},$$

$$x_2 = -\frac{2g}{M\Omega^2} + \frac{32\alpha_{\rm anh} g^3}{M^4\Omega^8}. \tag{3}$$

This asymmetric shift of the equilibrium phonon coordinate as a function of lattice anharmonicity causes two main effects: (1) The model loses particle-hole symmetry which allows a new type of superconductivity to emerge[14] and (2) the effective electron-electron attraction is sharply reduced as can be seen by a plot of the bipolaron binding energy in Fig. 2(b). Thus the lattice anharmonicity generates an effective *retarded* repulsive interaction between the electrons and breaks particle-hole symmetry, removing the nesting instability of the CDW at half filling and weak coupling. One expects that the lattice anharmonicity thereby to favor SC relative to CDW order, although it is also likely that anharmonic effects will reduce the transition temperatures (except close to the filled band, where the new hole-superconductivity mechanism can take over). What is surprising is that a rather small lattice anharmonicity can have a large effect on the electron-phonon problem.

Since the main effects of lattice anharmonicities are driven by the asymmetric distribution of the equilibrium phonon coordinate when there is zero, one, or two electrons on a lattice site, one expects that anharmonic effects will be strongest in the small-phonon-frequency limit. This is because the phonon coordinates all approach zero in the high-frequency limit (because the phonon reacts instantaneously to the change in the electrons) and these asymmetric effects disappear. Since phonon frequencies tend to be small in real materials, anharmonic effects can be important even if the phonon potential energy appears to be well approximated by a harmonic potential, i.e., if $\alpha_{\rm anh}$ is small.

Hirsch's new mechanism for superconductivity arises from an examination of the anharmonic electron-phonon model in the static limit.[14] The tunneling matrix element for a polaron from one lattice site to its nearest neighbor depends exponentially on the difference x_1-x_0 if there is no electron on the neighboring site and exponentially on x_2-x_1 if there is an electron occupying the neighboring site. The exponential dependence arises from the Franck-Condon overlap factors. Since these two values can be significantly different in an anharmonic model, one finds that the electronic motion will be dominated by a kinetic energy that depends on the density of the electrons at a given site. This is precisely the physical situation needed to generate superconductivity from kinetic energy effects—paired electrons have

a lower effective mass than a single electron, which induces the superconductivity transition at a low enough temperature. This novel mechanism for generating superconductivity has been analyzed via weak-coupling mean-field theory analyses[15] but has not yet been shown to exist in the exact solution of any model system. This mechanism for superconductivity disappears, however, in the strong-coupling limit where restriction is made to consider only empty sites and bipolarons. The single-electron (polaronic) states are integrated out because the bipolaron binding energy is much larger than the electronic hopping integral. Electron-hole symmetry is restored since these polaronic states only appear in virtual processes.

The anharmonicity has a much different effect than a direct electron-electron repulsion. The electron-electron repulsion uniformly reduces the bipolaron binding energy without changing the equilibrium phonon coordinates when there are zero, one, or two electrons at a lattice site. Thus, (1) the bipolaron binding energy can become negative (signifying that there is no electron-electron pairing) and (2) the system explicitly retains its electron-hole symmetry. Furthermore, since the repulsion is instantaneous, the retardation effects are unchanged from the case without Coulomb repulsion; i.e., the Franck-Condon overlaps remain the same. Thus we expect CDW ordering to always survive at half filling (if there is a net electron-electron attraction) and that both SC and CDW order will disappear as the Coulomb repulsion becomes too large, but it is not clear whether or not they disappear together or at different values of the electron-phonon coupling.

This contribution is a continuation of the work of one of the authors[9] on the strong-coupling expansion for the harmonic Holstein model to include both anharmonic and Coulomb repulsion effects. In Sec. II, the formalism for the perturbation theory and the generation of the effective pseudospin Hamiltonian will be described. In Sec. III, a mean-field-theory analysis of the pseudospin Hamiltonian will be given, and appropriate phase diagrams calculated for both the anharmonic case and the Coulomb repulsion case. Conclusions and a discussion will follow in Sec. IV.

II. FORMALISM FOR THE PERTURBATIVE ANALYSIS

The strong-coupling expansions are carried out with a method based on perturbation theory. The ground state is a bipolaronic state consisting of either paired electrons or empty sites. The distribution of these bipolarons is not determined to zeroth order in the electronic kinetic energy, and so the ground state is highly degenerate. The effective Hamiltonian (within this degenerate subspace) can be determined by using operator methods. In the late 1950s, Anderson[16] used such methods to show that the strong-interaction-strength limit of the Hubbard model is described by a Heisenberg antiferromagnet with an exchange integral $j=4|t_{ij}|^2/|U|$ that vanishes as the interaction strength increases. Kato[17] described how to determine the effective Hamiltonian for an arbitrary degenerate subspace using perturbation theory and operator methods. His analysis was applied to the Hubbard model in one dimension by Klein and Seitz[18] and in arbitrary dimensions by Takahashi[19] (see also the recent work by van Dongen[20]). Beni, Pincus, and Kanamori[21] and Hirsch and Fradkin[22] applied the same methods to the harmonic Holstein model determining the effective Hamiltonian to second order in the hopping. This analysis was extended to fourth order by Freericks.[9]

Kato's method[17] begins with a Hamiltonian $H=H_0+T$, with H_0 the unperturbed Hamiltonian and T the perturbation. In our case, H_0 corresponds to the Hamiltonian in Eq. (1) with $t_{ij}=0$, and the perturbation T is the electronic kinetic energy. The ground-state energy is E_0, Q_0 denotes the subspace that contains all of the degenerate ground states, and the projection operator onto Q_0 is P_0:

$$H_0P_0=P_0H_0=E_0P_0, \quad P_0^2=P_0. \tag{4}$$

As the perturbation is turned on, the eigenstates will evolve into a new subspace Q with corresponding projection operator P. If it is assumed that the subspace Q has a nonzero overlap with the unperturbed subspace Q_0, then the standard eigenvalue equation $(H-E)|E\rangle=0$ can be projected onto the unperturbed subspace Q_0, $P_0(H-E)PP_0|E\rangle=0$, to yield an effective equation for the perturbed eigenvalue E. The Hamiltonian P_0HPP_0 acts purely within the unperturbed subspace Q_0 and has an overlap operator P_0PP_0 that is not equal to the identity. Taking into account this nontrivial overlap results in an effective Hamiltonian of the form[23,9] $H_{\rm eff}=H_0+H_2+H_4+\cdots$, since only even powers of the perturbation enter for the generalized Holstein model. The first two nontrivial terms of the effective Hamiltonian satisfy

$$H_2:=P_0T\frac{1-P_0}{E_0-H_0}TP_0 \tag{5}$$

and

$$\begin{aligned} H_4:=&P_0T\frac{1-P_0}{E_0-H_0}T\frac{1-P_0}{E_0-H_0}T\frac{1-P_0}{E_0-H_0}TP_0 \\ &-\frac{1}{2}\left[P_0T\frac{1-P_0}{(E_0-H_0)^2}TP_0T\frac{1-P_0}{E_0-H_0}TP_0\right. \\ &\left.+P_0T\frac{1-P_0}{E_0-H_0}T\frac{1-P_0}{(E_0-H_0)^2}TP_0\right]. \end{aligned} \tag{6}$$

The expansion for the effective Hamiltonian can be expressed graphically by a set of diagrams. A solid line denotes virtual processes where an electron hops from site i to site j with strength t_{ij}. All diagrams must be closed, since the effective Hamiltonian acts solely within the degenerate subspace Q_0, implying that each virtually broken electron pair must be restored. There is only one possibility for the second-order term, which corresponds to either hopping from site i to site j and hopping back to site i or which corresponds to subsequent hops from site i to site j. The diagram that illustrates both of these processes is depicted in Fig. 1(a). There are four possible diagrams that contribute to fourth order which are also depicted in Fig. 1. The first three diagrams are linked diagrams which form nonvanishing contributions to the effective Hamiltonian. The last diagram 1(e) is an unlinked diagram which does not contribute to the effective Hamiltonian because the contributions from the positive and negative terms in Eq. (6) cancel. The unlinked dia-

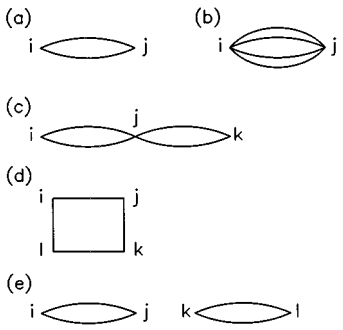

FIG. 1. Schematic diagrams used in the determination of the effective Hamiltonian. The second-order diagram is plotted in (a), while the fourth-order diagrams appear in (b)–(e). The fourth-order diagrams link two (b), three (c), or four (d) distinct lattice sites. The contributions from the unlinked diagram (e) vanish.

grams must cancel in order to have an energy per lattice site that is finite in the thermodynamic limit. The nonvanishing fourth-order terms fall into three categories: those that link two distinct sites [Fig. 1(b)], three distinct sites [Fig. 1(c)], or four distinct sites [Fig. 1(d)].

The matrix elements for the effective Hamiltonian are determined by introducing appropriate complete sets of states between each of the operator factors in Eqs. (5) and (6) for each of the possible intermediate virtual states summarized by the diagrams in Fig. 1. In the following section, thermodynamic phase transitions are determined from the effective Hamiltonian via a mean-field-theory analysis. An approximation is made here, that the transition temperature T_c is much smaller than the excitation energy of the lowest state above the ground state for the local anharmonic phonon with zero or two electrons on that site. In the harmonic case ($\alpha_{\rm anh}=0$), this excitation energy is Ω, and even in the anharmonic case, this excitation energy remains of the order of magnitude of Ω. If the transition temperature is much smaller than the excitation energy, then restriction can be made to the degenerate subspace Q_0 corresponding to the ground state of the phonons and one need not consider the effective Hamiltonian in the subspaces corresponding to excited phonon states. This is not a restrictive approximation, because the small-frequency limit is already known to be singular, since the degenerate subspace Q_0 becomes much larger when $\Omega=0$ than when $\Omega\neq 0$. Ω/t^* will be set equal to 0.5 for the numerical work in Sec. III.

Determination of the effective Hamiltonian proceeds in a similar fashion to the harmonic case.[21,22,9] The minimum of the anharmonic potential lies at x_0, x_1, and x_2 when there are zero, one, or two electrons, respectively, at a given lattice site (in the harmonic case we have $x_n=-ng/M\Omega^2$). Let $|+m\rangle$, $|m\rangle$, and $|-m\rangle$ denote the mth anharmonic oscillator state centered about the origin with zero, one, and two electrons, respectively, and E_m^+ E_m, and E_m^- denote the corresponding eigenvalues under the unperturbed Hamiltonian H_0. The overlaps $\langle \pm m|n\rangle$ will need to be calculated numerically in the general case. For the harmonic oscillator, a simple form is found:

$$\langle \pm m|n\rangle=\frac{1}{\sqrt{m!n!}}e^{-S/4}\langle 0|[a\pm\sqrt{S/2}]^m[a^\dagger\mp\sqrt{S/2}]^n|0\rangle. \tag{7}$$

Here $a^\dagger$ (a) is the harmonic-oscillator creation (annihilation) operator. In the harmonic case, one can use Eq. (7) to determine the parameters of the effective Hamiltonian analytically.

We will concentrate, however, on the anharmonic case, where the local phonon problem must be solved numerically. The unperturbed Hamiltonian H_0 consists of a collection of local phonon Hamiltonians, one for each lattice site, with a fixed number of electrons $n=0,1,2$ at each lattice site i. The local Hamiltonian is

$$H_{\rm loc}=\frac{1}{2M}p^2+\frac{1}{2}M\Omega^2x^2+\alpha_{\rm anh}x^4+gnx, \tag{8}$$

where we ignore terms that do not depend on the phonon coordinate or momentum. For harmonic phonons, the unit of length is (Planck's constant is set equal to 1) $x^*:=1/\sqrt{M\Omega}$. Reexpressing the Hamiltonian in terms of a dimensionless distance $y:=x/x^*$ yields

$$H_{\rm loc}=\frac{\Omega}{2}\overline{H}(n,y),\quad \overline{H}(n,y):=-\frac{d^2}{dy^2}+\overline{V}(n,y),$$

$$\overline{V}(n,y):=y^2+vy^4+wny, \tag{9}$$

with $v:=2\alpha_{\rm anh}/M^2\Omega^2$ and $w:=2g/\sqrt{m\Omega^3}$. The Schrödinger equation $H\phi_m=e(m)\phi_m$ is then solved numerically with the Numerov algorithm.[24] Schrödinger's equation is cast into a three term recursion relation which is iterated from the far left and from the far right, and matched at the middle. To start the iteration requires a good initial guess for the eigenvalue. This is provided by the WKBJ guess $e_{\rm WKBJ}(m)$ found from

$$2m+1=\frac{2}{\pi}\int dy\sqrt{e_{\rm WKBJ}(m)-\overline{V}(y)}. \tag{10}$$

We generally solve for the 30 lowest eigenvalues and eigenvectors in the sectors with zero, one, or two electrons.

The effective Hamiltonian is determined by evaluating all possible contributions from each of the nonvanishing diagrams in Fig. 1. Consider first the second-order term in Fig. 1(a). If both site i and site j are occupied by bipolarons, then the hopping matrix cannot connect the two sites by the Pauli principle. Similarly, if both sites are empty, there is no connection by the hopping term. It is only if one site is occupied by a bipolaron and the other site empty that the hopping matrix can connect through a virtual state back to the degenerate subspace. Consider the case with a bipolaron $\uparrow\downarrow$ at site i and an empty site 0 at site j. The hopping perturbation breaks the electron pair, with one electron hopping to site j and either hopping back to site i or the other electron also hops from site i to site j. Both processes are illustrated schematically below (with $\uparrow$ or $\downarrow$ corresponding to a single electron at a lattice site):

$$\uparrow\downarrow 0\Rightarrow\uparrow\downarrow\Rightarrow\uparrow\downarrow 0, \tag{11}$$

$$\uparrow\downarrow 0\Rightarrow\uparrow\downarrow\Rightarrow 0\uparrow\downarrow, \tag{12}$$

where only one of the two possible intermediate states is shown.

It is convenient to express the effective Hamiltonian in terms of pseudospin operators.[25] If the lattice is bipartite, so that it can be separated into A and B sublattices with nonzero hopping matrix elements only between sublattices A and B, then one can define pseudospin operators via

$$J_j^+ := (-1)^j c_{j\uparrow}^\dagger c_{j\downarrow}^\dagger, \quad J_j^- := (J_j^+)^\dagger,$$

$$J_j^z := \tfrac{1}{2}[n_{j\uparrow}+n_{j\downarrow}-1], \tag{13}$$

and the factor $(-1)^j$ is 1 for the A sublattice and (-1) for the B sublattice. The pseudospin operators satisfy an SU(2) algebra and form a spin-$\frac{1}{2}$ representation in the strong-coupling limit. A doubly occupied site corresponds to an up spin and an empty site corresponds to a down spin. The matrix elements of the effective Hamiltonian (that connects site i to site j) satisfy

$$\begin{aligned} H_2(i,j)|\uparrow\uparrow\rangle &= 0, \\ H_2(i,j)|\uparrow\downarrow\rangle &= -\tfrac{1}{2}j_\parallel^{(2)}(i,j)|\uparrow\downarrow\rangle + \tfrac{1}{2}j_\perp^{(2)}(i,j)|\downarrow\uparrow\rangle, \\ H_2(i,j)|\downarrow\uparrow\rangle &= -\tfrac{1}{2}j_\parallel^{(2)}(i,j)|\downarrow\uparrow\rangle + \tfrac{1}{2}j_\perp^{(2)}(i,j)|\uparrow\downarrow\rangle, \\ H_2(i,j)|\downarrow\downarrow\rangle &= 0, \end{aligned} \tag{14}$$

which is an XXZ Heisenberg antiferromagnet,

$$H_2 = \frac{1}{2}\sum_{i,j}\left\{ j_\perp^{(2)}(i,j)\frac{1}{2}\sum_a J_i^a J_j^{-a} + j_\parallel^{(2)}(i,j)\left[J_i^z J_j^z - \frac{1}{4}\right]\right\}, \tag{15}$$

where the index a runs over $+$ and $-$. Note that the summation is not restricted to $i<j$ (the overall factor of $\frac{1}{2}$ is introduced to compensate for double counting). Be careful not to confuse the pseudospin Hamiltonian from the original Hamiltonian that consists of bipolarons and empty sites.

The two parameters $j_\parallel^{(2)}$ and $j_\perp^{(2)}$ are determined by introducing complete sets of states into Eq. (5) for each of the virtual processes in Eqs. (11) and (12) and employing the definitions given in Eq. (14). The results are

$$j_\parallel^{(2)} = \sum_{m,n=0}^{\infty} 4t_{ij}^2 \frac{\langle -0|m\rangle\langle m|-0\rangle\langle +0|n\rangle\langle n|+0\rangle}{E_0^+ + E_0^- - E_m - E_n}, \tag{16}$$

$$j_\perp^{(2)} = \sum_{m,n=0}^{\infty} 4t_{ij}^2 \frac{\langle -0|m\rangle\langle m|+0\rangle\langle +0|n\rangle\langle n|-0\rangle}{E_0^+ + E_0^- - E_m - E_n}. \tag{17}$$

The fourth-order terms are all evaluated in a similar fashion. They can be separated into three different forms $H_4 = H_4(b) + H_4(c) + H_4(d)$ corresponding to the three different linked diagrams in Fig. 1. The effective Hamiltonian for each of these three cases takes the form

$$H_4(b) = \frac{1}{2}{\sum_{i,j}}' \left\{ j_\perp^{(4)}(i,j)\frac{1}{2}\sum_a J_i^a J_j^{-a} + j_\parallel^{(4)}(i,j)\left[J_i^z J_j^z - \frac{1}{4}\right]\right\}, \tag{18}$$

$$H_4(c) = \frac{1}{2}{\sum_{i,j,k}}' \left\{ j_\perp' \frac{1}{2}\sum_a [J_i^a J_j^{-a} + J_k^a J_j^{-a}] - j_\parallel'\left[J_i^z J_j^z + J_k^z J_j^z - \frac{1}{2}\right] + j_\perp'' \frac{1}{2}\sum_a J_i^a J_k^{-a} + [j_\parallel' + j_\parallel'']\left[J_i^z J_k^z - \frac{1}{4}\right]\right\}, \tag{19}$$

$$\begin{aligned} H_4(d) = \frac{1}{8}{\sum_{i,j,k,l}}' \Bigg\{ & \frac{\alpha}{2} + \frac{\delta}{4} + \frac{\nu}{8} - \frac{\nu}{2}[J_i^z J_j^z + J_i^z J_l^z + J_k^z J_j^z + J_k^z J_l^z] + \frac{\beta+\epsilon}{2}\sum_a [J_i^a J_j^{-a} + J_i^a J_l^{-a} + J_k^a J_j^{-a} + J_k^a J_l^{-a}] \\ & - \left(\delta - \frac{\nu}{2}\right)[J_i^z J_k^z + J_j^z J_l^z] + \frac{\gamma+\mu}{2}\sum_a [J_i^a J_k^{-a} + J_j^a J_l^{-a}] + 2(\beta-\epsilon)\sum_a [J_i^z J_j^z J_k^a J_l^{-a} + J_k^z J_l^z J_i^a J_j^{-a} \\ & + J_i^z J_l^z J_k^a J_j^{-a} + J_k^z J_j^z J_i^a J_l^{-a}] + 2(\gamma-\mu)\sum_a [J_i^z J_k^z J_j^a J_l^{-a} + J_j^z J_l^z J_i^a J_k^{-a}] + [-8\alpha + 4\delta + 2\nu] J_i^z J_j^z J_k^z J_l^z \\ & + \frac{\rho}{2}\sum_a \sum_b [J_i^a J_j^{-a} J_k^b J_l^{-b} + J_i^a J_l^{-a} J_k^b J_j^{-b} - J_i^a J_k^{-a} J_j^b J_l^{-b}] \Bigg\}, \end{aligned} \tag{20}$$

where the lattice-site-index dependence of the parameters has been suppressed, and the prime on the summations means that the sites i,j,k and i,j,k,l are all distinct (the overall factors of $\frac{1}{2}$ and $\frac{1}{8}$ are introduced to compensate for double counting). Explicit expressions for each of the parameters in Eqs. (18), (19), and (20) are given in the Appendix.

The effective pseudospin Hamiltonian is an anisotropic frustrated antiferromagnetic Heisenberg model with additional quartic spin-spin interactions.

The effect of the Coulomb repulsion is almost trivial. The Coulomb repulsion does not change any of the matrix elements; all it does is shift the energy of the bipolaron upward by U_C, $E_m^- \to E_m^- + U_C$, and so the effect of Coulomb repulsion can be included without much extra effort. One might

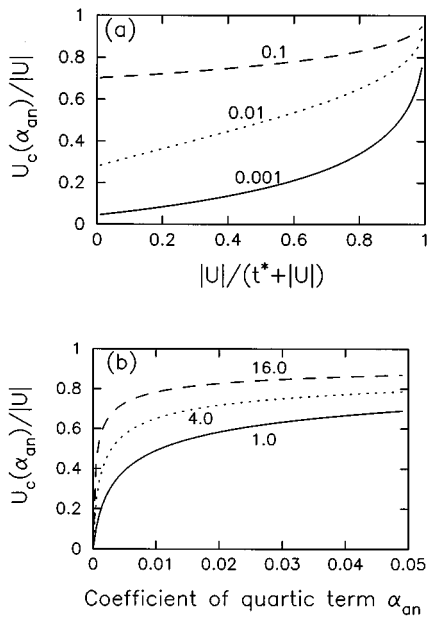

FIG. 2. Reduction of the bipolaron binding energy [which is the definition of $U_C(\alpha_{\rm anh})$] plotted as functions of the electron-phonon coupling (a) and the anharmonicity (b). In (a), three different values of the anharmonicity parameter are chosen: $\alpha_{\rm anh}=0.001$ (solid line), 0.01 (dotted line), and 0.1 (dashed line). Note how the reduction of the bipolaron binding energy increases with both $\alpha_{\rm anh}$ and U. In (b), the reduction in bipolaron binding energy is plotted as a function of $\alpha_{\rm anh}$ for three values of $|U|$: $|U|=1$ (solid line), $|U|=4$ (dotted line), and $|U|=16$ (dashed line). Note that even relatively small values of $\alpha_{\rm anh}$ produce a sharp reduction in the bipolaron binding energy.

try to approximate the effect of the anharmonicity by an instantaneous Coulomb repulsion, chosen to match the reduction of the bipolaron binding energy when the anharmonicity is included, i.e., define

$$U_C(\alpha_{\rm anh}):=E_0^-(\alpha_{\rm anh})+E_0^+(\alpha_{\rm anh})-2E_0(\alpha_{\rm anh})+|U|, \tag{21}$$

as the difference in the binding energy of the anharmonic bipolaron from the harmonic bipolaron. This reduction in bipolaron binding energy is plotted in Figs. 2(a) and 2(b) as a function of the harmonic bipolaron binding energy (for fixed values of $\alpha_{\rm anh}$) and as a function of $\alpha_{\rm anh}$ (for fixed values of U), respectively. Notice how even a small value of the anharmonicity produces a large reduction of the bipolaron binding energy and that the reduction increases as the electron-phonon interaction strength increases (the phonon frequency is fixed at $\Omega/t^*=0.5$).

III. MEAN-FIELD-THEORY ANALYSIS

We consider the case of hopping between nearest neighbors on a hypercubic lattice in d dimensions. The only nonzero matrix elements are then $t_{ij}=t^*/2\sqrt{d}$ when i and j are nearest neighbors. As described above, t^* is chosen to be the energy unit. This choice of scaling the hopping matrix elements inversely as the square root of the dimensionality is made so that the theory has a nontrivial limit[26] as $d\to\infty$.

We employ a mean-field-theory analysis to the pseudospin form of the effective Hamiltonian. Two types of phase transitions occur: (1) staggered order along the z axis [corresponding to CDW order at the ''antiferromagnetic'' $(\pi,\pi,\ldots)$ point] and (2) staggered order along the x axis (corresponding to SC order with a zero-momentum pair-field state). The mean-field theory becomes exact in high dimensions, and should provide an upper bound to the transition temperatures in finite dimensions (because nonlocal quantum fluctuations should reduce the transition temperature further).

The mean-field theory is constructed by determining the molecular field at each lattice site and equating the expectation value of the magnetization with that of a free spin in an external magnetic field equal to the molecular field, $\mathbf{h}_{\rm mol}$, yielding

$$\langle\mathbf{J}\rangle=\frac{\mathbf{h}_{\rm mol}}{|\mathbf{h}_{\rm mol}|}\,\frac{1}{2}\tanh\frac{1}{2}\beta|\mathbf{h}_{\rm mol}|, \tag{22}$$

as first described by Gorter.[27] The difficult part of the calculation involves a correct determination of the molecular field. One must be certain to properly count the contributions from each of the diagrams in Fig. 1. Note that the total number of distinct nearest-neighbor pairs corresponding to Figs. 1(a) and 1(b) is Nd, with N the number of lattice sites, and each pair appears twice in the unrestricted summations. There are two classes of second-neighbor diagrams corresponding to Fig. 1(c): those where j and k are not parallel [of the $(1,1,0,\ldots)$ form] and those where j and k are parallel [of the $(2,0,0,\ldots)$ form]. In the first case, there are $Nd(d-1)$ pairs, with each pair appearing 4 times in the unrestricted summation. In the second case, there are Nd pairs, with each pair appearing twice in the unrestricted summation. Finally there are $\frac{1}{2}Nd(d-1)$ distinct squares corresponding to Fig. 1(d) with each square appearing 8 times in the unrestricted summation. Using these results, it is a straightforward exercise to rewrite the Hamiltonian as a summation over distinct pairs (and squares) and then extract the molecular fields for the corresponding ordered phases.

A hypercubic lattice is bipartite and so it divides into two sublattices A and B, where the nearest-neighbor hopping occurs only from sublattice A to sublattice B or vice versa. The paramagnetic high-temperature phase corresponds to a uniform magnetization of the pseudospins on each sublattice:

$$\langle\mathbf{J}_A\rangle=\langle\mathbf{J}_B\rangle=:\tfrac{1}{2}m\mathbf{e}_z=\tfrac{1}{2}(\rho_e-1)\mathbf{e}_z, \tag{23}$$

where $\mathbf{e}_z$ is the unit vector along the z axis and ρ_e is the electron concentration. The self-consistent equation for the pseudospin magnetization becomes

$$m=\tanh\tfrac{1}{2}\beta\Bigg\{2(\mu-U)+md\Bigg[-j_\parallel^{(2)}-j_\parallel^{(4)}+(2d-1)(j_\parallel'-j_\parallel'')+(d-1)\left(\delta+\frac{1}{2}\nu\right)\Bigg]+m^3d(d-1)[2\alpha-\delta-\tfrac{1}{2}\nu]\Bigg\}. \tag{24}$$

The dependence of the chemical potential μ upon the electron concentration ρ_e can easily be determined by inverting Eq. (24).

The transition temperature to the commensurate charge-density-wave phase occurs at a temperature where the pseudospin magnetization satisfies

$$\langle \mathbf{J}_A \rangle = \tfrac{1}{2}(m+m')\mathbf{e}_z, \quad \langle \mathbf{J}_B \rangle = \tfrac{1}{2}(m-m')\mathbf{e}_z, \tag{25}$$

in the limit $m' \to 0$. We only consider the transition to a commensurate CDW, because transitions to incommensurate phases can only occur if the frustration induced by the fourth-order terms in the effective Hamiltonian becomes large enough. Since the validity of the truncated strong-coupling expansion fails when the fourth-order terms are comparable in size to the second-order terms, we ignore the complication of incommensurate order here.

The transition temperature is then easily found to be

$$\begin{aligned} T_c = \tfrac{1}{2}\rho_e(2-\rho_e)\{ & dj_\parallel^{(2)} - d^2[6j_\parallel' + 2j_\parallel'' - \delta + \tfrac{3}{2}\nu \\ & + (2\alpha - \delta - \tfrac{1}{2}\nu)(1-\rho_e)^2] + d[j_\parallel^{(4)} + 3j_\parallel' + j_\parallel'' - \delta + \tfrac{3}{2}\nu \\ & + (2\alpha - \delta - \tfrac{1}{2}\nu)(1-\rho_e)^2]\}. \end{aligned} \tag{26}$$

Note that this expression differs slightly (in the coefficient of the δ term) from that given previously,[9] and corrects a typographical error in that work. Explicit formulas for the parameters appearing in Eq. (26) appear in the Appendix.

Likewise, the superconducting transition temperature is determined by finding the temperature where the pseudospin magnetization satisfies

$$\langle J_A^z \rangle = \langle J_B^z \rangle = \tfrac{1}{2}m, \quad \langle J_A^x \rangle = -\langle J_B^x \rangle = \tfrac{1}{2}m', \tag{27}$$

in the limit $m' \to 0$. The transition temperature is

$$\begin{aligned} T_c = \frac{\rho_e - 1}{\ln[\rho_e/(2-\rho_e)]}\{ & dj_\perp^{(2)} + d^2[4j_\perp' - 2j_\perp'' + 2\beta - \gamma + 2\epsilon - \mu \\ & + (2\beta - \gamma - 2\epsilon + \mu)(1-\rho_e)^2] + d[j_\perp^{(4)} - 2j_\perp' + j_\perp'' - 2\beta \\ & + \gamma - 2\epsilon + \mu + (-2\beta + \gamma + 2\epsilon - \mu)(1-\rho_e)^2]\}. \end{aligned} \tag{28}$$

Explicit formulas for the parameters appearing in Eq. (28) appear in the Appendix.

The above expressions for the transition temperatures to CDW or SC order are evaluated below in the infinite dimensional limit. In this case, there is no contribution from the fourth-order terms that are multiplied by a linear power in d, because they scale like $t^{*4}/d \to 0$ in the large-dimensional limit.

At half-filling ($\rho_e = 1$), the CDW phase is expected to be the ground state if either the anharmonicity or the Coulomb repulsion is not too large. Figure 3 plots the CDW transition temperature at half filling for different values of the anharmonicity [Fig. 3(a)] and the Coulomb repulsion [Fig. 3(b)]. Both the second-order approximations (which monotonically diverge as the interaction strength approaches zero) and the fourth-order approximations (which properly show a peak in T_c as a function of the coupling) are plotted. In Fig. 3(a), four different values of the anharmonicity are shown: $\alpha_{\rm anh} = 0.0$ (the harmonic case) (solid line), $\alpha_{\rm anh} = 0.001$ (dotted line), $\alpha_{\rm anh} = 0.005$ (dashed line), and $\alpha_{\rm anh} = 0.015$ (dash-dotted line). It is apparent that even though the second-order approximation shows large enhancements to the transition temperature as the anharmonicity is increased, the fourth-order approximation indicates that the maximal CDW transition temperature actually decreases as the anharmonicity increases. Furthermore, the value of coupling strength where the maximum occurs increases as a function of anharmonicity. This is to be expected since the anharmonicity acts in some respects like a retarded Coulomb repulsion. What is surprising is that relatively small values of anharmonicity have such large effects on the transition temperature.

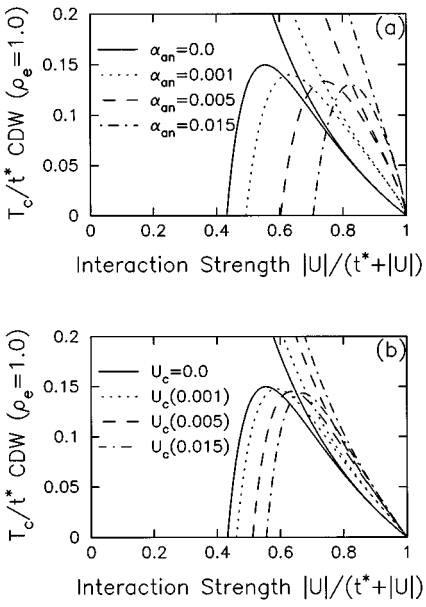

FIG. 3. Charge-density-wave transition temperature at half filling for the anharmonic Holstein model (a) or the Holstein-Hubbard model (b). Both second-order and fourth-order approximations are plotted (the fourth-order approximations have a peak in T_c). Note that the maximal T_c for the fourth-order calculation decreases as either the anharmonicity or Coulomb repulsion is turned on. In (a), the anharmonicity varies from $\alpha_{\rm anh} = 0.0$ (solid line), $\alpha_{\rm anh} = 0.001$ (dotted line), $\alpha_{\rm anh} = 0.005$ (dashed line), and $\alpha_{\rm anh} = 0.015$ (dash-dotted line). In (b), the Coulomb repulsion is chosen to match the reduction in the bipolaron binding energy for each value of the anharmonicity plotted in (a), i.e., $U_C = U_C(\alpha_{\rm anh})$ with $\alpha_{\rm anh} =$ 0.0, 0.001, 0.005, and 0.015. Note that the effect of anharmonicity is not easily mimicked by Coulomb repulsion except for the smallest values of $\alpha_{\rm anh}$.

In Fig. 3(b), the CDW transition temperature at half filling is plotted for four different values of $U_C(\alpha_{\rm anh})$. The same values of $\alpha_{\rm anh}$ are used as in Fig. 3(a). Note that once again the maximal T_c decreases as $\alpha_{\rm anh}$ increases (implying that U_C increases). Furthermore, the peak does not move as rapidly to larger values of the coupling strength, indicating that the retardation effects are rather strong even at the relatively large phonon frequency of $\Omega/t^* = 0.5$.

Note that these strong coupling phase diagrams may be more accurate than those of the harmonic model, because it

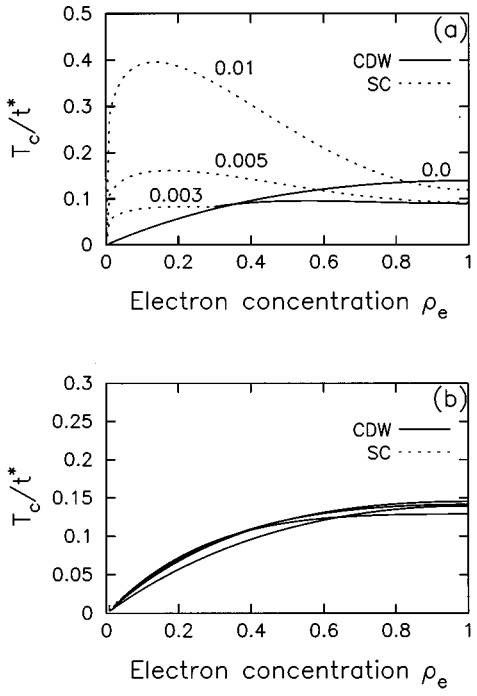

FIG. 4. Phase diagram of the anharmonic Holstein model (a) and the Holstein-Hubbard model (b) for $|U|=1.5625$ corresponding to the peak in the charge-density-wave transition temperature at half filling for the harmonic Holstein model. The solid lines denote charge-density-wave transition temperatures and the dotted lines denote superconducting transition temperatures. In (a), the anharmonicity strength assumes four values $\alpha_{\rm anh}=0.0$, 0.003, 0.005, and 0.01. Note that the anharmonicity strongly enhances superconducting solutions relative to charge-density-wave solutions, and if $\alpha_{\rm anh}$ is large enough, there is no CDW order. Note furthermore, that the maximal superconducting T_c is larger than the maximal CDW T_c in the harmonic case and occurs at a rather low value of the electron filling. In (b), the Coulomb repulsion is fixed to be $U_C(\alpha_{\rm anh})$ with $\alpha_{\rm anh}$ the same as in (a). Note that the effect of the Coulomb repulsion on the transition temperatures is relatively minor, and the strong enhancement of the superconducting T_c does not occur.

is known that in the case of either an anharmonic interaction or a Coulomb repulsion that the CDW instability only occurs when the coupling strength U is large enough in magnitude. Hence the true T_c does vanish at a finite value of U, as it does in the fourth-order approximation.

Our analysis at half filling has ignored the possibility of SC order. In fact, the system will go superconducting at half filling in the regime where the CDW transition temperature has been suppressed to zero, but since this regime corresponds to a region where the fourth-order approximations are breaking down, we have not complicated Fig. 3 by including the superconducting solutions at small $|U|$. Rather, we examine what happens as the system is doped away from half-filling. In Fig. 4, the phase diagram is plotted for the coupling strength $U=-1.5625t^*$ which lies at the peak of the CDW transition temperature curve when $\alpha_{\rm anh}=0$. This case represents a lower limit of applicability of the strong-coupling expansion. In Fig. 4(a), the anharmonicity varies from $\alpha_{\rm anh}=0$, 0.003, 0.005, and 0.01. The solid lines denote CDW solutions, and the dotted lines are SC. Note that the CDW-SC phase boundary lies at exponentially small densities in the harmonic case. As the anharmonicity is turned on, the CDW transition temperature is suppressed, and the SC transition temperature is enhanced; so the CDW-SC phase boundary moves in towards half filling. When $\alpha_{\rm anh}=0.005$, the CDW phase has disappeared. The enhancement of the SC transition temperature continues as $\alpha_{\rm anh}$ increases, until it is significantly larger than the maximal CDW transition temperature of the harmonic Holstein model. Hence, the strong coupling approximation, through fourth order, predicts a large enhancement in the SC transition temperature relative to the harmonic case. It is not clear whether this result is an artifact of the approximation or is a real effect. Note further that the electron density where the maximal superconducting T_c occurs is near the band edges. This is similar in spirit to Hirsch's mechanism, but, as far as we can tell, is unrelated, because in the strong coupling limit the effect occurs both at the top and the bottom of the band, since the approximation explicitly retains electron-hole symmetry.

In Fig. 4(b), the same phase diagrams are plotted, this time using $U_C(\alpha_{\rm anh})$ with the same values of $\alpha_{\rm anh}$ as in Fig. 4(a). Clearly one can see that the effect of the Coulomb repulsion is quite different from the anharmonicity. The phase diagram does not change much, and the large enhancement of T_c in the SC channel does not occur.

In order to check to see whether these results are generic or occur simply because one is close to the limiting region where the approximations are expected to hold, we have also calculated the phase diagrams for a stronger value of the interaction strength $U=-4.0t^*$. In Fig. 5(a), four different values of $\alpha_{\rm anh}$ (0.0, 0.01, 0.03, and 0.05) are plotted. Here the results are similar to those found in Fig. 4, except the anharmonicity initially causes the CDW T_c to rise, because of the reduction in the bipolaron binding energy. The SC transition temperature still has a large maximum at low densities and is significantly enhanced relative to the harmonic case. Furthermore, the CDW-SC phase boundary continues to move toward half-filling until it disappears at $\alpha_{\rm anh}\approx 0.03$. In Fig. 5(b), we plot the same phase diagrams, this time using $U_C(\alpha_{\rm anh})$. Once again, the phase diagram displays very different behavior, with the CDW-SC phase transition remaining at exponentially small densities.

Finally, we study how the critical electron density, where the CDW-SC phase boundary lies, evolves as functions of U and $\alpha_{\rm anh}$. In the anharmonic Holstein model, we see in Fig. 6(a) that the phase boundary moves very rapidly as the anharmonicity is turned on. This indicates how the anharmonicity strongly favors SC solutions relative to CDW order. In Fig. 6(b), we show the analogous plots of the critical electron density for the harmonic Holstein-Hubbard model, with U_C chosen from Eq. (21), and the same values of $\alpha_{\rm anh}$. Clearly the anharmonic behavior is not easily mimicked by an instantaneous Coulomb repulsion, and the retardation effects cannot be neglected.

IV. CONCLUSIONS

The strong-coupling expansion for the anharmonic Holstein-Hubbard model has been presented through fourth order in the hopping. This result extends the analysis of the harmonic case.[9] We find some interesting results from this analysis. First, the anharmonicity reduces the bipolaron bind-

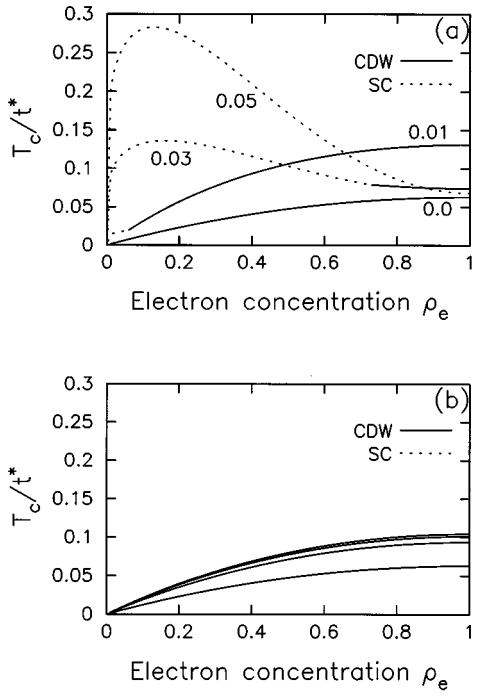

FIG. 5. Phase diagram of the anharmonic Holstein model (a) and the Holstein-Hubbard model (b) for $|U|=4.0$. The solid lines denote charge-density-wave transition temperatures and the dotted lines denote superconducting transition temperatures. In (a), the anharmonicity strength assumes four values $\alpha_{\rm anh}=0.0$, 0.01, 0.03, and 0.05. Note that the large enhancement in the superconducting T_c is seen here too (although it occurs at a larger value of the anharmonicity). In (b), the Coulomb repulsion is fixed to be $U_C(\alpha_{\rm anh})$ with $\alpha_{\rm anh}$ the same as in (a). Once again, the effect of Coulomb repulsion is drastically different from that of the anharmonicity.

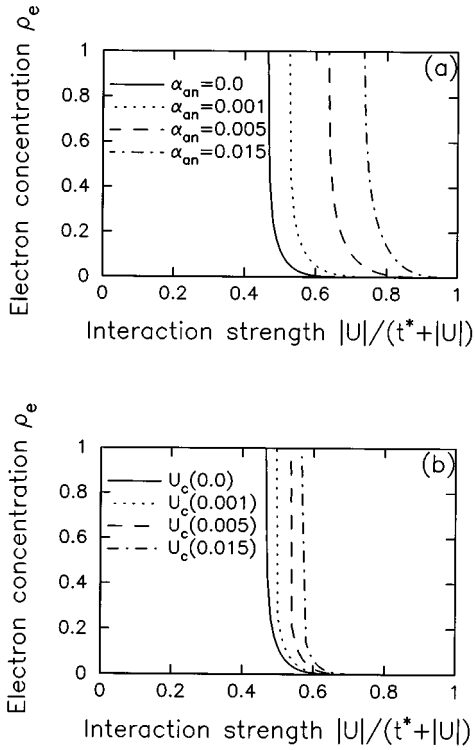

FIG. 6. Plot of the charge-density-wave–superconductor phase boundary as functions of electron concentration and U. In (a), the phase diagram is plotted for the anharmonic Holstein model with $\alpha_{\rm anh}=0.0$ (solid line), 0.001 (dotted line), 0.005 (dashed line), and 0.015 (dash-dotted line). In Fig. 6(b), the phase diagram is plotted for the Holstein-Hubbard model with $U_C=U_C(\alpha_{\rm anh})$ and $\alpha_{\rm anh}$ chosen to have the same values as in (a). These figures show that the anharmonicity strongly favors superconductivity relative to CDW order, much more so than turning on a Coulomb repulsion.

ing energy and, second, it reduces the equilibrium phonon-coordinate spacing between one electron at a site and either zero or two electrons at a site. The first effect is expected to cause an enhancement to transition temperatures in the strong-coupling regime, and the second should enhance the Franck-Condon overlap factors for superconducting order, favoring the SC phase relative to the CDW. Similarly, a Coulomb repulsion will reduce the bipolaron binding energy, but does not alter the Franck-Condon overlaps. We find that in the CDW phase, the maximal transition temperature actually decreases when either anharmonicity or Coulomb repulsion is turned on. For the superconducting phase, the enhancement of the Franck-Condon overlap factors (equivalent to a widening of the polaron band) causes a large enhancement of the SC transition temperature at low electron density, even for moderate values of the anharmonicity. In no case do we find that the effect of the anharmonicity is easily mimicked by an effective Coulomb repulsion.

Since the strong-coupling expansion is expected to fail in both the low-electron-concentration regime and when the effective bipolaron binding energy is no longer much larger than the hopping integral, it is possible that this large enhancement of the superconducting transition temperature is just an artifact of the current approximation. It is important to compare these approximations to exact quantum Monte Carlo simulations of the transition temperatures of the anharmonic Holstein model. Work in this direction is currently in progress.

ACKNOWLEDGMENTS

We would like to acknowledge useful conversations with J. Hirsch and M. Jarrell. J.K.F. acknowledges The Petroleum Research Fund, administered by the American Chemical Society, for partial support of this research (ACS-PRF No. 29623-GB6) and an Oak Ridge Associated University Junior Faculty Enhancement Award for partial support of this research. G.D.M. acknowledges support by the University of Tennessee, and by Oak Ridge National Laboratory, managed by Lockheed Martin Energy Research Corporation for the U.S. Department of Energy under Contract No. DE-AC05-96OR22464.

APPENDIX: PARAMETERS OF THE FOURTH-ORDER EFFECTIVE PSEUDOSPIN HAMILTONIAN

In this appendix explicit expressions are given for the parameters that appear in the fourth-order effective pseudospin Hamiltonian, summarized in Eqs. (18), (19), and (20). The notation used is that given in the text.

First the parameters in Eq. (18) (an overall factor of t_{ij}^4 is suppressed):

$$j_{\parallel}^{(4)}=-8\Bigg\{\sum_{\substack{l,l',m,m',n,n'=0\\ m+m'\neq 0}}^{\infty}\Bigg[\frac{\langle+0|n\rangle\langle n|+m\rangle\langle+m|l\rangle\langle l|+0\rangle\langle-0|n'\rangle\langle n'|-m'\rangle\langle-m'|l'\rangle\langle l'|-0\rangle}{[E_0^+ +E_0^- -E_n-E_{n'}][E_0^+ +E_0^- -E_m^+ -E_{m'}^-][E_0^+ +E_0^- -E_l-E_{l'}]}$$

$$+\frac{\langle+0|n\rangle\langle n|-m\rangle\langle-m|l\rangle\langle l|+0\rangle\langle-0|n'\rangle\langle n'|+m'\rangle\langle+m'|l'\rangle\langle l'|-0\rangle}{[E_0^+ +E_0^- -E_n-E_{n'}][E_0^+ +E_0^- -E_m^+ -E_{m'}^-][E_0^+ +E_0^- -E_l-E_{l'}]}\Bigg]$$

$$-\sum_{l,l',n,n'=0}^{\infty}\Bigg[\frac{\langle+0|n\rangle\langle n|+0\rangle\langle-0|n'\rangle\langle n'|-0\rangle\langle+0|l\rangle\langle l|+0\rangle\langle-0|l'\rangle\langle l'|-0\rangle}{[E_0^+ +E_0^- -E_n-E_{n'}]^2[E_0^+ +E_0^- -E_l-E_{l'}]}$$

$$+\frac{\langle+0|n\rangle\langle n|-0\rangle\langle-0|n'\rangle\langle n'|+0\rangle\langle-0|l\rangle\langle l|+0\rangle\langle+0|l'\rangle\langle l'|-0\rangle}{[E_0^+ +E_0^- -E_n-E_{n'}]^2[E_0^+ +E_0^- -E_l-E_{l'}]}\Bigg]\Bigg\}, \tag{A1}$$

$$j_{\perp}^{(4)}=-8\Bigg\{\sum_{\substack{l,l',m,m',n,n'=0\\ m+m'\neq 0}}^{\infty}\Bigg[\frac{\langle+0|n\rangle\langle n|+m\rangle\langle+m|l\rangle\langle l|-0\rangle\langle-0|n'\rangle\langle n'|-m'\rangle\langle-m'|l'\rangle\langle l'|+0\rangle}{[E_0^+ +E_0^- -E_n-E_{n'}][E_0^+ +E_0^- -E_m^+ -E_{m'}^-][E_0^+ +E_0^- -E_l-E_{l'}]}$$

$$+\frac{\langle+0|n\rangle\langle n|-m\rangle\langle-m|l\rangle\langle l|-0\rangle\langle-0|n'\rangle\langle n'|+m'\rangle\langle+m'|l'\rangle\langle l'|+0\rangle}{[E_0^+ +E_0^- -E_n-E_{n'}][E_0^+ +E_0^- -E_m^+ -E_{m'}^-][E_0^+ +E_0^- -E_l-E_{l'}]}\Bigg]$$

$$-\sum_{l,l',n,n'=0}^{\infty}\Bigg[\frac{\langle+0|n\rangle\langle n|+0\rangle\langle-0|n'\rangle\langle n'|-0\rangle\langle+0|l\rangle\langle l|-0\rangle\langle-0|l'\rangle\langle l'|+0\rangle}{[E_0^+ +E_0^- -E_n-E_{n'}]^2[E_0^+ +E_0^- -E_l-E_{l'}]}$$

$$+\frac{\langle+0|n\rangle\langle n|-0\rangle\langle-0|n'\rangle\langle n'|+0\rangle\langle-0|l\rangle\langle l|-0\rangle\langle+0|l'\rangle\langle l'|+0\rangle}{[E_0^+ +E_0^- -E_n-E_{n'}]^2[E_0^+ +E_0^- -E_l-E_{l'}]}\Bigg]\Bigg\}. \tag{A2}$$

Next the parameters in Eq. (19) (an overall factor of $t_{ij}^2 t_{jk}^2$ is suppressed):

$$j_{\parallel}'=4\Bigg\{\sum_{l,l',m,n,n'=0}^{\infty}\frac{\langle+0|n\rangle\langle n|+0\rangle\langle-0|n'\rangle\langle n'|+m\rangle\langle+m|l'\rangle\langle l'|-0\rangle\langle+0|l\rangle\langle l|+0\rangle}{[E_0^+ +E_0^- -E_n-E_{n'}][2E_0^+ +E_0^- -E_m^+ -E_n-E_l]}\Bigg[\frac{1}{E_0^+ +E_0^- -E_l-E_{l'}}$$

$$+\frac{1}{E_0^+ +E_0^- -E_n-E_{l'}}\Bigg]+2\sum_{\substack{l,l',n,n'=0\\ m\neq 0}}^{\infty}\frac{\langle+0|n\rangle\langle n|+0\rangle\langle-0|n'\rangle\langle n'|-m\rangle\langle-m|l'\rangle\langle l'|-0\rangle\langle+0|l\rangle\langle l|+0\rangle}{[E_0^+ +E_0^- -E_n-E_{n'}][E_0^+ -E_m^+][E_0^+ +E_0^- -E_l-E_{l'}]}$$

$$-2\sum_{l,l',n,n'=0}^{\infty}\frac{\langle+0|n\rangle\langle n|+0\rangle\langle-0|n'\rangle\langle n'|-0\rangle\langle-0|l'\rangle\langle l'|-0\rangle\langle+0|l\rangle\langle l|+0\rangle}{[E_0^+ +E_0^- -E_n-E_{n'}]^2[E_0^+ +E_0^- -E_l-E_{l'}]}\Bigg\}, \tag{A3}$$

$$j_{\parallel}''=-4\sum_{l,l',m,n,n'=0}^{\infty}\frac{\langle+0|n\rangle\langle n|+m\rangle\langle+m|l'\rangle\langle l'|+0\rangle\langle-0|n'\rangle\langle n'|-0\rangle\langle+0|l\rangle\langle l|+0\rangle}{[E_0^+ +E_0^- -E_n-E_{n'}][2E_0^+ +E_0^- -E_m^+ -E_l-E_{n'}][E_0^+ +E_0^- -E_{l'}-E_{n'}]}, \tag{A4}$$

$$j'_\perp = -4\Bigg\{ \sum_{l,l',m,n,n'=0}^{\infty} \frac{\langle +0|n\rangle\langle n|+0\rangle\langle -0|n'\rangle\langle n'|+m\rangle\langle +m|l'\rangle\langle l'|+0\rangle\langle +0|l\rangle\langle l|-0\rangle}{[E_0^+ + E_0^- - E_n - E_{n'}][2E_0^+ + E_0^- - E_m^+ - E_n - E_l]} \Bigg[\frac{1}{E_0^+ + E_0^- - E_l - E_{l'}}$$

$$+ \frac{1}{E_0^+ + E_0^- - E_n - E_{l'}} \Bigg] + 2 \sum_{\substack{l,l',n,n'=0 \\ m\neq 0}}^{\infty} \frac{\langle +0|n\rangle\langle n|+0\rangle\langle -0|n'\rangle\langle n'|-m\rangle\langle -m|l'\rangle\langle l'|+0\rangle\langle +0|l\rangle\langle l|-0\rangle}{[E_0^+ + E_0^- - E_n - E_{n'}][E_0^+ - E_m^+][E_0^+ + E_0^- - E_l - E_{l'}]}$$

$$- \sum_{l,l',n,n'=0}^{\infty} \frac{\langle +0|n\rangle\langle n|+0\rangle\langle -0|n'\rangle\langle n'|-0\rangle\langle -0|l'\rangle\langle l'|+0\rangle\langle +0|l\rangle\langle l|-0\rangle}{[E_0^+ + E_0^- - E_n - E_{n'}][E_0^+ + E_0^- - E_l - E_{l'}]} \Bigg[\frac{1}{E_0^+ + E_0^- - E_n - E_{n'}}$$

$$+ \frac{1}{E_0^+ + E_0^- - E_l - E_{l'}} \Bigg] \Bigg\}, \tag{A5}$$

$$j''_\perp = 4\Bigg\{ \sum_{l,l',m,n,n'=0}^{\infty} \frac{\langle +0|n\rangle\langle n|+m\rangle\langle +m|l'\rangle\langle l'|+0\rangle\langle -0|n'\rangle\langle n'|+0\rangle\langle +0|l\rangle\langle l|-0\rangle}{[E_0^+ + E_0^- - E_n - E_{n'}][2E_0^+ + E_0^- - E_m^+ - E_{n'} - E_l][E_0^+ + E_0^- - E_l - E_{l'}]}$$

$$+ 2 \sum_{\substack{l,l',n,n'=0 \\ m\neq 0}}^{\infty} \frac{\langle +0|n\rangle\langle n|-m\rangle\langle -m|l'\rangle\langle l'|+0\rangle\langle -0|n'\rangle\langle n'|+0\rangle\langle +0|l\rangle\langle l|-0\rangle}{[E_0^+ + E_0^- - E_n - E_{n'}][E_0^+ - E_m^+][E_0^+ + E_0^- - E_l - E_{l'}]}$$

$$- 2 \sum_{l,l',n,n'=0}^{\infty} \frac{\langle +0|n\rangle\langle n|-0\rangle\langle -0|n'\rangle\langle n'|+0\rangle\langle -0|l'\rangle\langle l'|+0\rangle\langle +0|l\rangle\langle l|-0\rangle}{[E_0^+ + E_0^- - E_n - E_{n'}]^2[E_0^+ + E_0^- - E_l - E_{l'}]} \Bigg\}. \tag{A6}$$

Finally the parameters in Eq. (20) (an overall factor of $t_{ij}t_{jk}t_{kl}t_{ki}$ is suppressed):

$$\alpha = 4 \sum_{l,l',n,n'=0}^{\infty} \frac{\langle +0|n\rangle\langle n|+0\rangle\langle -0|n'\rangle\langle n'|-0\rangle\langle +0|l\rangle\langle l|+0\rangle\langle +0|l'\rangle\langle l'|+0\rangle}{[E_0^+ + E_0^- - E_n - E_{n'}][E_0^+ + E_0^- - E_l - E_{n'}][E_0^+ + E_0^- - E_{l'} - E_{n'}]}, \tag{A7}$$

$$\beta = -2 \sum_{l,l',n,n'=0}^{\infty} \Bigg\{ \frac{\langle +0|n\rangle\langle n|-0\rangle\langle -0|n'\rangle\langle n'|+0\rangle\langle +0|l\rangle\langle l|+0\rangle\langle +0|l'\rangle\langle l'|+0\rangle}{[E_0^+ + E_0^- - E_n - E_{n'}][E_0^+ + E_0^- - E_l - E_n][E_0^+ + E_0^- - E_{l'} - E_n]}$$

$$+ \frac{\langle +0|n\rangle\langle n|+0\rangle\langle -0|n'\rangle\langle n'|+0\rangle\langle +0|l\rangle\langle l|+0\rangle\langle +0|l'\rangle\langle l'|-0\rangle}{E_0^+ + E_0^- - E_n - E_{n'}} \Bigg[\frac{1}{[E_0^+ + E_0^- - E_{l'} - E_n][E_0^+ + E_0^- - E_l - E_{l'}]}$$

$$+ \frac{1}{[E_0^+ + E_0^- - E_l - E_{n'}][E_0^+ + E_0^- - E_l - E_{l'}]} + \frac{1}{[E_0^+ + E_0^- - E_l - E_{n'}][E_0^+ + E_0^- - E_{l'} - E_{n'}]} \Bigg] \Bigg\}, \tag{A8}$$

$$\gamma = 4 \sum_{l,l',n,n'=0}^{\infty} \Bigg\{ \frac{\langle +0|n\rangle\langle n|+0\rangle\langle -0|n'\rangle\langle n'|+0\rangle\langle +0|l\rangle\langle l|-0\rangle\langle +0|l'\rangle\langle l'|+0\rangle}{[E_0^+ + E_0^- - E_n - E_{n'}][E_0^+ + E_0^- - E_l - E_{n'}][E_0^+ + E_0^- - E_l - E_{l'}]}$$

$$+ \frac{\langle +0|n\rangle\langle n|+0\rangle\langle -0|n'\rangle\langle n'|+0\rangle\langle +0|l\rangle\langle l|+0\rangle\langle +0|l'\rangle\langle l'|-0\rangle}{[E_0^+ + E_0^- - E_n - E_{n'}][E_0^+ + E_0^- - E_l - E_n]} \Bigg[\frac{1}{E_0^+ + E_0^- - E_{l'} - E_n} + \frac{1}{E_0^+ + E_0^- - E_l - E_{l'}} \Bigg] \Bigg\}, \tag{A9}$$

$$\delta = -4 \sum_{l,l',n,n'=0}^{\infty} \Bigg\{ \frac{\langle +0|n\rangle\langle n|+0\rangle\langle -0|n'\rangle\langle n'|-0\rangle\langle +0|l\rangle\langle l|+0\rangle\langle -0|l'\rangle\langle l'|-0\rangle}{[E_0^+ + E_0^- - E_n - E_{n'}][E_0^+ + E_0^- - E_l - E_{n'}][E_0^+ + E_0^- - E_l - E_{l'}]}$$

$$+ \frac{\langle +0|n\rangle\langle n|+0\rangle\langle -0|n'\rangle\langle n'|-0\rangle\langle -0|l\rangle\langle l|-0\rangle\langle +0|l'\rangle\langle l'|+0\rangle}{[E_0^+ + E_0^- - E_n - E_{n'}][E_0^+ + E_0^- - E_l - E_n][E_0^+ + E_0^- - E_l - E_{l'}]} \Bigg\}, \tag{A10}$$

$$\epsilon=2\sum_{l,l',n,n'=0}^{\infty}\left\{2\frac{\langle+0|n\rangle\langle n|-0\rangle\langle-0|n'\rangle\langle n'|+0\rangle\langle+0|l\rangle\langle l|+0\rangle\langle-0|l'\rangle\langle l'|-0\rangle}{[E_0^+ +E_0^- -E_n-E_{n'}][2E_0^+ +2E_0^- -E_n-E_{n'}-E_l-E_{l'}]}\left[\frac{1}{E_0^+ +E_0^- -E_{l'}-E_{n'}}\right.\right.$$
$$\left.+\frac{1}{E_0^+ +E_0^- -E_l-E_n}\right]+\frac{\langle+0|n\rangle\langle n|+0\rangle\langle-0|n'\rangle\langle n'|-0\rangle\langle+0|l\rangle\langle l|-0\rangle\langle-0|l'\rangle\langle l'|+0\rangle}{[E_0^+ +E_0^- -E_n-E_{n'}][E_0^+ +E_0^- -E_l-E_{n'}]}\left[\frac{1}{E_0^+ +E_0^- -E_{l'}-E_{n'}}\right.$$
$$\left.+\frac{1}{E_0^+ +E_0^- -E_l-E_{l'}}\right]+\frac{\langle+0|n\rangle\langle n|+0\rangle\langle-0|n'\rangle\langle n'|-0\rangle\langle-0|l\rangle\langle l|+0\rangle\langle+0|l'\rangle\langle l'|-0\rangle}{[E_0^+ +E_0^- -E_n-E_{n'}][E_0^+ +E_0^- -E_l-E_n]}\left[\frac{1}{E_0^+ +E_0^- -E_{l'}-E_n}\right.$$
$$\left.\left.+\frac{1}{E_0^+ +E_0^- -E_l-E_{l'}}\right]\right\}, \tag{A11}$$

$$\mu=-2\sum_{l,l',n,n'=0}^{\infty}\left\{2\frac{\langle+0|n\rangle\langle n|-0\rangle\langle-0|n'\rangle\langle n'|-0\rangle\langle+0|l\rangle\langle l|+0\rangle\langle-0|l'\rangle\langle l'|+0\rangle}{[E_0^+ +E_0^- -E_n-E_{n'}][2E_0^+ +2E_0^- -E_n-E_{n'}-E_l-E_{l'}]}\left[\frac{1}{E_0^+ +E_0^- -E_{l'}-E_{n'}}\right.\right.$$
$$\left.+\frac{1}{E_0^+ +E_0^- -E_l-E_n}\right]+\frac{\langle+0|n\rangle\langle n|-0\rangle\langle-0|n'\rangle\langle n'|+0\rangle\langle-0|l\rangle\langle l|+0\rangle\langle+0|l'\rangle\langle l'|+0\rangle}{[E_0^+ +E_0^- -E_n-E_{n'}][E_0^+ +E_0^- -E_l-E_n][E_0^+ +E_0^- -E_{l'}-E_n]}$$
$$\left.+\frac{\langle+0|n\rangle\langle n|+0\rangle\langle-0|n'\rangle\langle n'|+0\rangle\langle+0|l\rangle\langle l|-0\rangle\langle-0|l'\rangle\langle l'|-0\rangle}{[E_0^+ +E_0^- -E_n-E_{n'}][E_0^+ +E_0^- -E_l-E_{n'}][E_0^+ +E_0^- -E_{l'}-E_{n'}]}\right\}, \tag{A12}$$

$$\nu=-8\sum_{l,l',n,n'=0}^{\infty}\left\{\frac{\langle+0|n\rangle\langle n|+0\rangle\langle-0|n'\rangle\langle n'|-0\rangle\langle+0|l\rangle\langle l|+0\rangle\langle-0|l'\rangle\langle l'|-0\rangle}{[E_0^+ +E_0^- -E_n-E_{n'}][2E_0^+ +2E_0^- -E_n-E_{n'}-E_l-E_{l'}]}\left[\frac{1}{E_0^+ +E_0^- -E_{l'}-E_n}\right.\right.$$
$$\left.\left.+\frac{1}{E_0^+ +E_0^- -E_l-E_{n'}}\right]\right\}, \tag{A13}$$

$$\rho=-8\sum_{l,l',n,n'=0}^{\infty}\left\{\frac{\langle+0|n\rangle\langle n|-0\rangle\langle-0|n'\rangle\langle n'|+0\rangle\langle+0|l\rangle\langle l|-0\rangle\langle-0|l'\rangle\langle l'|+0\rangle}{[E_0^+ +E_0^- -E_n-E_{n'}][2E_0^+ +2E_0^- -E_n-E_{n'}-E_l-E_{l'}]}\left[\frac{1}{E_0^+ +E_0^- -E_l-E_{l'}}\right.\right.$$
$$\left.+\frac{1}{E_0^+ +E_0^- -E_n-E_{n'}}\right]+\frac{\langle+0|n\rangle\langle n|-0\rangle\langle-0|n'\rangle\langle n'|+0\rangle\langle-0|l\rangle\langle l|+0\rangle\langle+0|l'\rangle\langle l'|-0\rangle}{[E_0^+ +E_0^- -E_n-E_{n'}][E_0^+ +E_0^- -E_l-E_{n'}]}\left[\frac{1}{E_0^+ +E_0^- -E_l-E_{l'}}\right.$$
$$\left.+\frac{1}{E_0^+ +E_0^- -E_{l'}-E_{n'}}\right]+\frac{\langle+0|n\rangle\langle n|-0\rangle\langle-0|n'\rangle\langle n'|+0\rangle\langle+0|l\rangle\langle l|-0\rangle\langle-0|l'\rangle\langle l'|+0\rangle}{[E_0^+ +E_0^- -E_n-E_{n'}][E_0^+ +E_0^- -E_l-E_n]}\left[\frac{1}{E_0^+ +E_0^- -E_{l'}-E_n}\right.$$
$$\left.\left.+\frac{1}{E_0^+ +E_0^- -E_l-E_{l'}}\right]\right\}. \tag{A14}$$

[1] A. B. Migdal, Zh. Eksp. Teor. Fiz. **34**, 1438 (1958) [Sov. Phys. JETP **7**, 999 (1958)].

[2] G. M. Eliashberg, Zh. Eksp. Teor. Fiz. **38**, 966 (1960) [Sov. Phys. JETP **11**, 696 (1960)].

[3] G. Liebfried and W. Ludwig, in *Solid State Physics*, edited by F. Seitz and D. Turnbull (Academic, New York, 1961), Vol. 12, p. 75.

[4] H. Horner, in *Dynamical Properties of Solids*, edited by G. K. Horton and A. A. Maradudin (North-Holland, Amsterdam, 1974), Vol. 1, p. 451.

[5] J. A. Reissland, *The Physics of Phonons* (Wiley, New York, 1973).

[6] J. C. K. Hui and P. B. Allen, J. Phys. F **4**, L42 (1974); A. E. Kavakozov and E. G. Maksimov, Zh. Eksp. Teor. Fiz. **74**, 681 (1978) [Sov. Phys. JETP **47**, 358 (1978)]; G. D. Mahan and J. O. Sofo, Phys. Rev. B **47**, 8050 (1993).

[7] J. K. Freericks and E. H. Lieb, Phys. Rev. B **51**, 2812 (1995).

[8] S. Robaszkiewicz, R. Micnas, and K. A. Chao, Phys. Rev. B **23**, 1447 (1981); A. S. Alexandrov, J. Ranninger, and S. Robaszkiewicz, *ibid.* **33**, 4526 (1986); R. Micnas, J. Ranninger, and S. Robaszkiewicz, Rev. Mod. Phys. **62**, 113 (1990).

[9] J. K. Freericks, Phys. Rev. B **48**, 3881 (1993).

[10] T. Holstein, Ann. Phys. (N.Y.) **8**, 325 (1959).

[11] J. Hubbard, Proc. R. Soc. London Ser. A **276**, 238 (1963); **277**, 237 (1964); **281**, 401 (1964); **285**, 542 (1965); **296**, 82 (1967).

[12] J. K. Freericks, M. Jarrell, and D. J. Scalapino, Phys. Rev. B **48**, 6302 (1993); J. K. Freericks, M. Jarrell, and D. J. Scalapino, Europhys. Lett. **25**, 37 (1994); J. K. Freericks and M. Jarrell, in *Computer Simulation Studies in Condensed Matter Physics VII*, edited by D. P. Landau, K. K. Mon, and H.-B. Schüttler

(Springer-Verlag, Berlin, 1995).
[13] J. K. Freericks and M. Jarrell, Phys. Rev. Lett. **75**, 2570 (1995).
[14] J. E. Hirsch, Phys. Rev. B **47**, 5351 (1993); F. Marsiglio and J. E. Hirsch, *ibid.* **49**, 1366 (1994).
[15] J. E. Hirsch and F. Marsiglio, Phys. Rev. B **39**, 11 515 (1989).
[16] P. W. Anderson, Phys. Rev. **115**, 2 (1959).
[17] T. Kato, Prog. Theor. Phys. **4**, 514 (1949).
[18] D. J. Klein and W. A. Seitz, Phys. Rev. B **8**, 2236 (1973).
[19] M. Takahashi, J. Phys. C **10**, 1289 (1977).
[20] P. G. J. van Dongen, Phys. Rev. B **49**, 7904 (1994).
[21] G. Beni, P. Pincus, and J. Kanamori, Phys. Rev. B **10**, 1896 (1974).
[22] J. E. Hirsch and E. Fradkin, Phys. Rev. Lett. **49**, 402 (1982); Phys. Rev. B **27**, 4302 (1983).
[23] P. O. Löwdin, J. Chem. Phys. **18**, 365 (1950); Adv. Phys. **5**, 1 (1956).
[24] G. D. Mahan and K. R. Subbaswamy, *Local Density Theory of Polarizability* (Plenum, New York, 1990).
[25] O. J. Heilmann and E. H. Lieb, Trans. N.Y. Acad. Sci. **33**, 116 (1971); C. N. Yang, Phys. Rev. Lett. **63**, 2144 (1989); M. Pernici, Europhys. Lett. **12**, 75 (1989); S. Zhang, Phys. Rev. Lett. **65**, 120 (1990).
[26] W. Metzner and D. Vollhardt, Phys. Rev. Lett. **62**, 324 (1989).
[27] C. J. Gorter, Rev. Mod. Phys. **25**, 277 (1953).